Renewable Energy 253 (2025) 123616

Contents lists available at ScienceDirect

Renewable Energy

journal homepage: www.elsevier.com/locate/renene

A modeling study of ocean thermal energy conversion resource and potential environmental effects around Kailua-Kona, Hawaii

Kyungmin Park [a], Zhaoqing Yang [a,b,*], Andrea E. Copping [a], Fadia Ticona Rollano [a]

[a] Coastal Sciences Division, Pacific Northwest National Laboratory, Seattle, WA, 98109, USA

[b] Department of Civil and Environmental Engineering, University of Washington, Seattle, WA, 98195, USA

ARTICLE INFO

Keywords:
Ocean thermal energy conversion (OTEC)
Marine energy
High-resolution numerical model
Temperature variability
Resource characterization
Hawaii

ABSTRACT

Ocean Thermal Energy Conversion (OTEC) offers a promising renewable energy solution using the temperature difference between warm surface seawater and cold deep seawater. Because detailed resource characterization is critical for the optimal design and implementation of OTEC systems, a high-resolution numerical model is employed to better characterize the OTEC resource at Kailua-Kona, Hawaii. The model results reveal distinct patterns and dynamics not captured by existing observations or low-resolution models. These findings highlight the importance of using high-resolution models for fine-scale predictions of thermal gradient variability, ultimately supporting more efficient and sustainable OTEC deployment. Additionally, the study investigates the impacts of mixed water discharge from OTEC plants that can alter ocean conditions and potentially destabilize the water column. Understanding these effects is vital for minimizing any potential negative environmental consequences and ensuring the long-term viability of OTEC operations. Our model improves OTEC resource characterization, which can lead to optimal design and deployment of OTEC systems. The analysis of OTEC water discharge impacts can accelerate the development of OTEC technologies, overcoming permitting/consenting challenges. These findings contribute to the broader adoption of high-resolution modeling in ocean energy resource characterization, particularly for OTEC applications.

1. Introduction

The oceans cover more than 70 % of the Earth's surface, making them the world's largest solar energy collector and storage system [1,2]. Ocean Thermal Energy Conversion (OTEC) is a technology that utilizes the difference in ocean temperatures over depth to generate electricity, providing an abundant and stable renewable energy resource [2–4]. For example, the 66-year mean estimates (from 1955 to 2021) of global OTEC power potential reach up to 9.4 TW [5]. In addition, unlike other renewable technologies based on intermittent energy sources such as wind and solar [6,7], OTEC can provide consistent baseload power [8–10]. These facts make OTEC a promising renewable energy technology.

There are two major types of OTEC systems: closed- and open-cycle systems [1,2]. Closed-cycle OTEC systems use low-boiling-point fluids such as ammonia. The warm surface water vaporizes a working fluid; then, the resulting vapor runs a turbine to generate electricity. The used vapor is then condensed with cold deep water. The condensed working fluid is pumped back into the evaporator to repeat the cycle. It remains in a closed system and circulates continuously. In an open-cycle OTEC system, the warm seawater is the working fluid. The warm seawater is evaporated in a low-pressure chamber to produce distilled water as steam. The steam expands through a turbine that is coupled to a generator to produce electricity. After that, the steam is condensed by cold seawater pumped from the ocean's depths. A membrane desalination system can be coupled with an open-cycle system to provide fresh water. In addition to conventional OTEC systems, recent technological advancements have explored diverse power conversion and integration strategies aimed at enhancing efficiency, adaptability, and multifunctionality. For example, Kalina cycle systems that utilize ammonia-water mixtures offer improved thermal efficiency over traditional Rankine cycles because of their ability to exploit variable boiling points [11]. Radial-inflow turbines have also been incorporated into OTEC designs, leveraging their compact configuration and high performance under low-temperature gradients [12]. Furthermore, OTEC is increasingly being developed for multipurpose applications beyond

This article is part of a special issue entitled: Ocean Energy Resource 2024 published in Renewable Energy.

* Corresponding author. Coastal Sciences Division, Pacific Northwest National Laboratory, Seattle, WA, 98109, USA.
E-mail address: zhaoqing.yang@pnnl.gov (Z. Yang).

https://doi.org/10.1016/j.renene.2025.123616
Received 7 August 2024; Received in revised form 19 May 2025; Accepted 29 May 2025
Available online 30 May 2025

electricity generation, including seawater desalination [13,14], absorption refrigeration [15], aquaculture [16], and deep seawater air conditioning [17]. These applications expand OTEC's role in supporting water supply, thermal management, and food security in island and coastal regions. Concurrently, there is growing emphasis on dynamic modeling and advanced control strategies to ensure stable and efficient OTEC operation under varying thermal and oceanographic conditions [18]. These developments collectively underscore the increasing complexity of OTEC systems and their dependence on accurate environmental data. In addition, successful OTEC operation is determined by several factors such as the temperature difference between surface warm water and deep cold water, the proximity to the coast, the bathymetry slope, smooth seafloor, the wave height, and the wind speed [19–21]. These conditions are highly variable over location and time. As a result, high-resolution resource characterization becomes important not only to optimize system design and ensure operational reliability, but also to inform site selection, assess environmental impacts, and evaluate long-term feasibility under changing ocean conditions.

Numerical models are beneficial for assessing OTEC power resources because they have several key advantages over observations. Numerical models can simulate extensive and remote ocean areas, which are often impractical and expensive to survey directly with observations. This capability is essential for evaluating the feasibility of OTEC systems at a global scale [5,10,22–24] to local-scale marine environments [19,21,25,26], allowing for assessments of potential sites without the geographic and logistic constraints associated with direct observation. In addition, unlike direct observations that provide data for a specific moment or short period, numerical models can project future scenarios and analyze long-term trends. This is particularly valuable for understanding seasonal to interannual variability [19] and the impacts of climate change on OTEC performance over decades [5]. These models help in forecasting future energy outputs and strategizing the sustainable development of OTEC facilities. Numerical models can also be used to perform experiments with various environmental and operational parameters. This includes adjusting water temperatures, flow rates, and turbine efficiencies to explore different outcomes for OTEC operations [4,10]. Numerical experiments are also instrumental in conducting environmental impact assessments and predicting ecological risks such as changes in marine ecosystems due to altered temperature, salinity, and nutrient concentrations by OTEC discharges [26–29]. Such flexibility is crucial for optimizing energy extraction processes and for planning under various environmental scenarios. The advantages of numerical models support the development of environmentally sustainable and economically viable OTEC projects.

Nevertheless, the OTEC resource characterizations for many coastal and island regions are still limited because high-resolution numerical models have not been thoroughly applied [21]. The limitations include poor representation of bathymetric features and local ocean dynamic features (e.g., upwelling and localized currents). In addition, coarse-resolution models face challenges when capturing oceanic mesoscale eddies, which can cause evident errors in the simulated ocean thermal stratification in the deeper ocean [30,31]. Therefore, the OTEC power, which is significantly affected by the temperature differential over depth, might not be accurately captured by a coarse-resolution model. Furthermore, a site-specific investigation of OTEC resources with a high-resolution model is a good approach for a better understanding of the OTEC system because geographical constraints and localized ocean conditions affect the economic and environmental aspects of OTEC operation [27,32].

In this context, the Hawaiian Islands offer an ideal case study for demonstrating the value of high-resolution modeling in OTEC resource characterization. The region's oceanographic conditions are highly favorable for OTEC deployment with strong and persistent thermal stratification characterized by warm surface waters overlaying cold deep waters. This steep and reliable temperature gradient is essential for maximizing the thermal efficiency of OTEC systems. From 2003 to 2018, approximately 84 %–90 % of the state's electricity was generated from petroleum, and petroleum products accounted for nearly 60 % of total imports [33]. This heavy dependence on imported fossil fuels increases vulnerability to supply disruptions and price volatility, underscoring the critical need for locally sourced, renewable energy alternatives that can enhance long-term energy security and sustainability. Recognizing Hawaii's potential for OTEC, Makai Ocean Engineering developed and has operated the first U.S. grid-connected OTEC demonstration plant (∼105 kW) in Kailua-Kona since 2015, providing a proof-of-concept for practical system deployment in the region [8]. However, despite this early success, previous modeling studies lacked the high-resolution information needed to evaluate site-specific resource variability, vertical structure, and environmental conditions critical for larger-scale OTEC implementation. Moreover, the ocean temperatures around Hawaii are strongly modulated by large-scale climate variabilities [34]. Three dominant climate modes that influence regional ocean conditions are the El Niño–Southern Oscillation (ENSO), the Pacific Decadal Oscillation (PDO) and the North Pacific Gyre Oscillation (NPGO). ENSO drives inter-annual variabilities in sea surface temperatures (SSTs) and stratification across the tropical Pacific, with widespread climate teleconnections [35]. The PDO modulates the decadal background state of the North Pacific and can interact with ENSO signals [36], while the NPGO influences salinity, nutrient transport, and subsurface thermal anomalies through gyre-scale circulation [37]. Despite their known influence on ocean conditions, the potential impacts of these climate modes on OTEC power generation in Kailua-Kona have not been assessed.

This study addresses the knowledge gaps by leveraging a high-resolution (up to 350 m) numerical model to evaluate the OTEC resource, its climate sensitivity and the impacts of OTEC operation on ocean conditions around Kailua-Kona, Hawaii. Comparisons of the model results with various observations validate the accuracy of the temperature characteristics for the 10-year record from 2012 to 2021. With the confidence of the model results, the high-resolution data provide better resource characterizations of OTEC, overcoming the lack of information from observations and coarse-resolution models in the target area.

The details of the numerical model and OTEC power calculation are presented in Section 2. We demonstrate the temperature characteristics and OTEC power in Section 3. The conclusions of this work are detailed in Section 4.

2. Methodology

2.1. Unstructured grid model SCHISM

The Semi-implicit Cross-scale Hydroscience Integrated System Model (SCHISM) is an open-source, 3D baroclinic model that utilizes unstructured grids. The source code is publicly available through GitHub (https://github.com/schism-dev/schism). This model features a flexible horizontal grid and integrates Localized Sigma Coordinates with Shaved Cells (LSC^2), allowing for variable vertical grids that adapt to the underlying bathymetry [38]. The versatile SCHISM grid system is designed for efficient cross-scale modeling, spanning from the open ocean to complex coastlines. SCHISM utilizes a semi-implicit Galerkin finite-element methodology to solve the Navier–Stokes equations with the hydrostatic and Boussinesq approximations. Within its advanced numerical framework, the model employs a semi-implicit scheme to handle the barotropic pressure gradient and vertical viscosity. In contrast, the baroclinic pressure gradient and horizontal viscosity are managed using an explicit scheme. For the temperature and salinity transport equations in this study, the third-order Weighted Essentially Non-Oscillatory (WENO) transport scheme is used, which is useful for multiscale baroclinic modeling [39]. To maintain strict conservation of volume and scalar quantities, SCHISM utilizes finite-volume solvers for the 3D continuity and scalar transport equations. Additionally, turbulent processes are modeled using the Generic Length Scale (GLS) model [40], further enhancing the model's accuracy and robustness.

The model is applied to a domain that encompasses the entire west coast of Hawaii Island (The Big Island) and extends to a water depth of 4800 m within the exclusive economic zone (EEZ). Fig. 1 illustrates the model domain with interpolated bathymetry and the computational mesh. The mesh is constructed based on the Digital Elevation Model (DEM) to accurately capture the bathymetry characteristics around Kailua-Kona, Hawaii. ETOPO 2022 data are utilized for mesh generation and bathymetry interpolation without any bathymetry treatment, such as smoothing. The inherent stability and robustness of SCHISM enable the use of original, unsmoothed bathymetries from the DEMs, thereby enhancing the fidelity and accuracy of the simulations [41]. The resulting mesh consists of 3161 nodes and 6133 elements, with a horizontal resolution varying from 4.5 km at the open boundary to 350 m around the Kona coast, where potential OTEC plants might be considered. The LSC^2 vertical grid system allows for a varying number of vertical layers, ranging from 1 in shallow waters to 48 in deeper oceans with higher density in the upper 500 m to better capture the thermocline structure.

A uniform bottom roughness length of 0.005 m is prescribed across the modeling domain. Wind stress calculations were performed based on the algorithm proposed by Hwang [42]. Tidal forcing is obtained from FES2014 [43]. The tidal model provides tidal components for the open boundary conditions and as a body force in the momentum equation, incorporating eight significant tidal constituents such as K1, K2, M2, N2, O1, P1, Q1, and S2. Boundary conditions such as the sea surface height, 3D water temperature, salinity, and currents are derived from the Copernicus Marine Environment Monitoring Service (CMEMS) [44]. Surface forcings, including wind velocities, atmospheric pressure, air temperature, and precipitation, utilize outputs from various atmospheric models such as the Climate Forecast System (CFS) v2 [45].

This study analyzes the temperature characteristics and OTEC powers for 10 years from 2012 to 2021. Because the time period

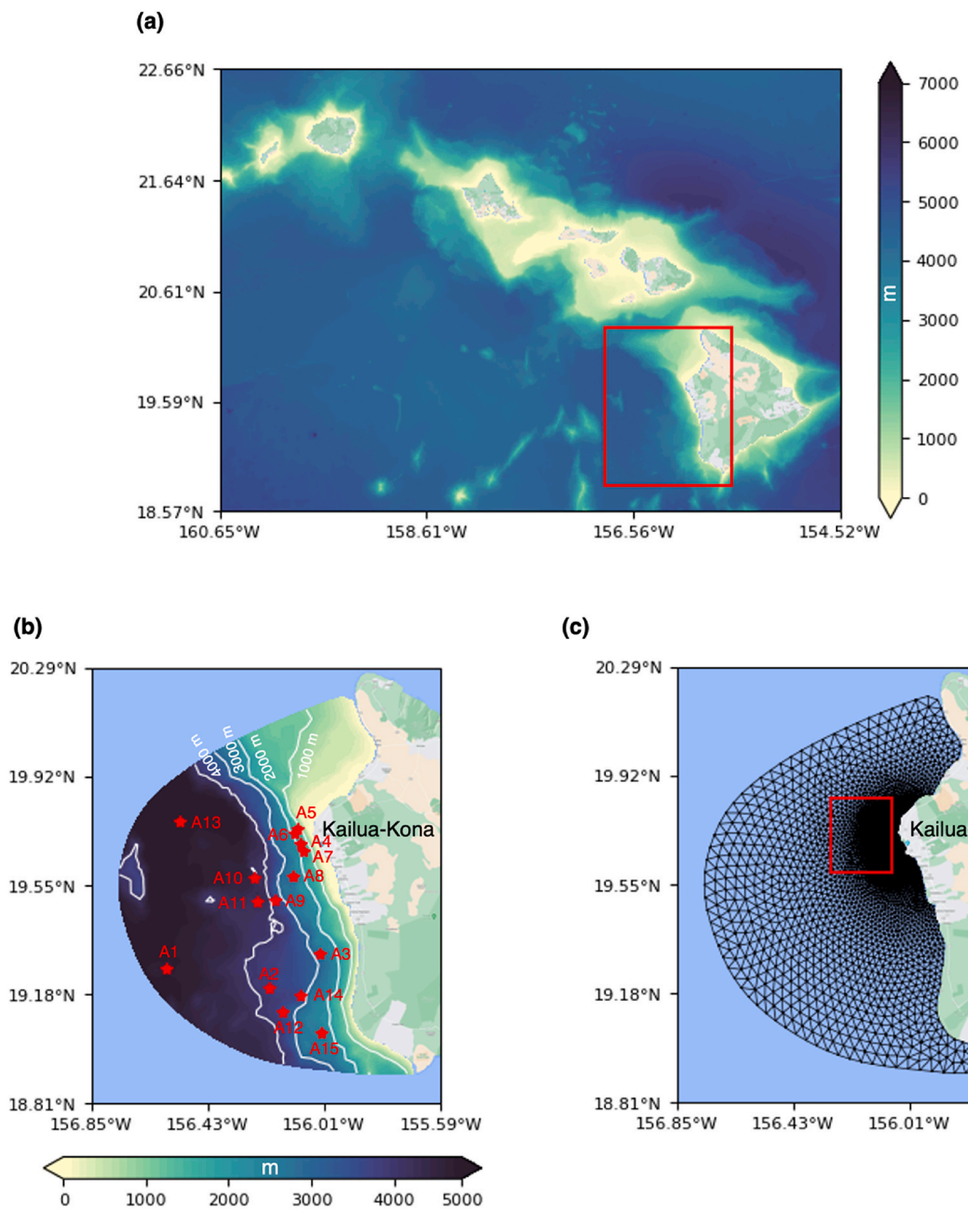

Fig. 1. (a) Hawaii island archipelago. The red box indicates the targeted area for the model development. (b) View of the model domain around Kailua-Kona, Hawaii, with interpolated bathymetry. The red stars indicate the locations of the Argo float observations used in Fig. 2. The white lines represent the bathymetric contour lines from 1000 m to 4000 m. (c) The computational mesh. The red box indicates the area used to calculate the spatially averaged sea surface temperature in Fig. 3. (For interpretation of the references to color in this figure legend, the reader is referred to the Web version of this article.)

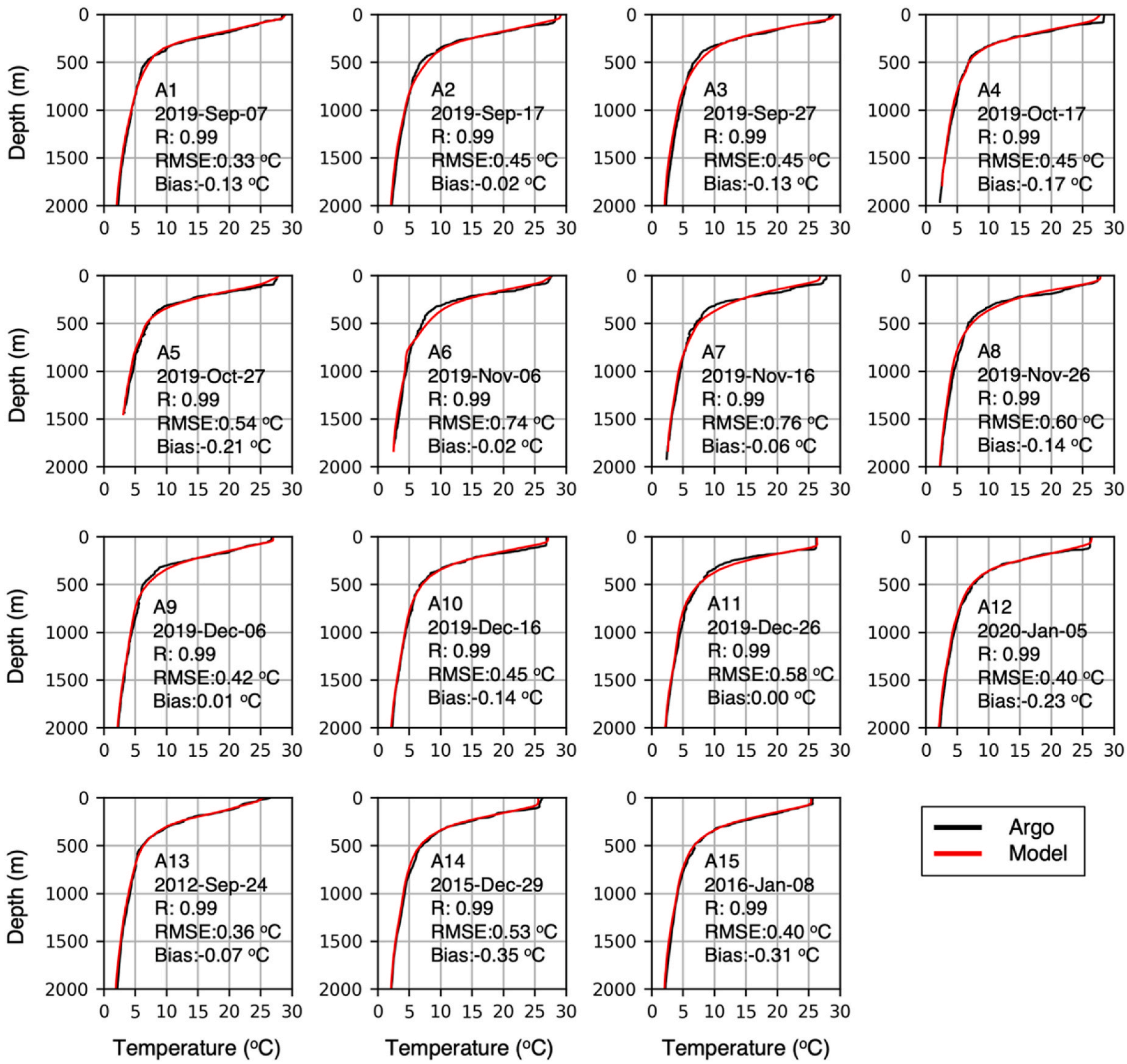

Fig. 2. Comparisons of the vertical profiles of the temperatures from Argo observations (black lines) and the model (red lines). The locations of the Argo floats are indicated in Fig. 1(a). The Argo float's index, measurement date, correlation coefficient (R), Root-mean-squared error (RMSE), and bias are presented in each panel. (For interpretation of the references to color in this figure legend, the reader is referred to the Web version of this article.)

represents the impact of large-scale climate variability, e.g., the NPGO, ENSO, and PDO on ocean temperatures in Hawaii [34], we investigate how the temperature variability caused by the climate phenomena affects OTEC power generation in the target area.

2.2. Observations and model validation

We evaluate and validate model results by comparison with different types of observational data, including Argo floats and satellites for vertical profiles of ocean temperatures and sea surface temperatures (SSTs). In this study, we utilize the following statistics to quantify model errors against the observations as follows:

Bias:

$$\frac{1}{N}\sum_{1}^{N}(M_i - O_i) \tag{1}$$

Root-mean-squared error (RMSE):

$$\sqrt{\frac{1}{N}\sum_{1}^{N}(M_i - O_i)^2} \tag{2}$$

Pearson correlation coefficient R:

$$\frac{\sum_{1}^{N}(M_i - \overline{M})(O_i - \overline{O})}{\sqrt{\sum_{1}^{N}(M - \overline{M})^2(O_i - \overline{O})^2}} \tag{3}$$

where M_i, O_i, N, $\overline{M}$, and $\overline{O}$ are the modeled values, observed values, number of samples, and means of the modeled and observed values, respectively.

The bias quantifies the average discrepancy between modeled and observed values, serving as an indicator of systematic overestimation or underestimation by the model. The RMSE measures the magnitude of the discrepancies between modeled and observed values, offering insights into the model's overall precision. R spans from -1, indicating a strong negative correlation, to 1, denoting a strong positive correlation. These three statistics are used in the model assessment Section 3.

2.3. OTEC power calculation

The OTEC power can be estimated as gross and net power [23,46,47]. In this study, we utilize the net OTEC power that takes into account the power consumed by an OTEC operation. The resulting formulation of the net OTEC power P_{net} is as follows:

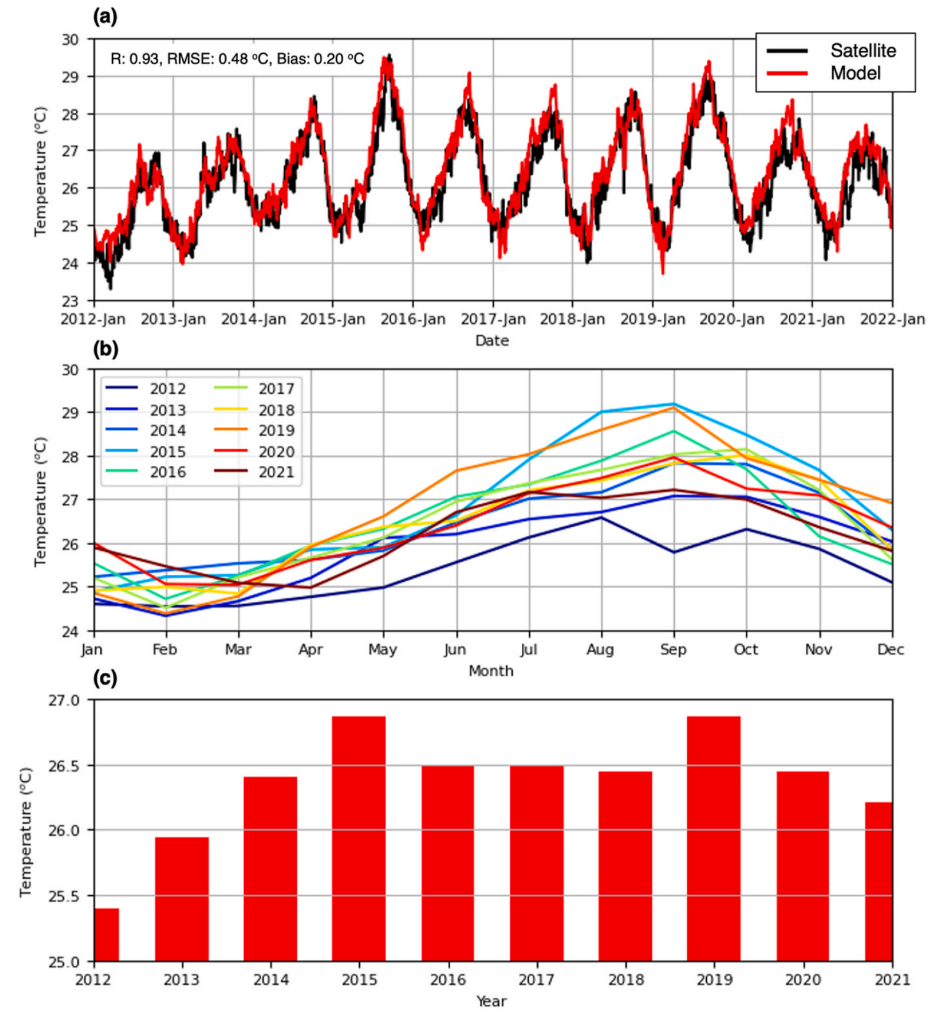

Fig. 3. (a) Time histories of spatial mean SST (seven-day running mean) from the satellite observation (black line) and model (red line) within the domain outlined in Fig. 1(c). (b) Monthly SST climatology for each year over the study period. (c) Bar graph of the annual mean SST derived from the time-series data in panel (a). (For interpretation of the references to color in this figure legend, the reader is referred to the Web version of this article.)

$$P_{\text{net}} = \frac{Q_{\text{cw}}\rho c_P \varepsilon_{\text{tg}}}{8T_{\text{surf}}}\left\{\frac{3\gamma}{2(1+\gamma)}\Delta T^2 - 0.18\Delta T^2_{\text{design}} - 0.12\left(\frac{\gamma}{2}\right)^{2.75}\Delta T^2_{\text{design}}\right\} \tag{4}$$

where $\rho = 1025\ \text{kg/m}^3$ is the average seawater density, $c_P \approx 4\ \text{kJ}/(\text{kg}\cdot\text{K})$ is the specific heat of the seawater, and $\gamma = Q_{\text{ww}}/Q_{\text{cw}}$ is the ratio of the warm surface water (Q_{ww} of 450 m^3/s) to cold deep water (Q_{cw} of 300 m^3/s) flow rates used in a 100 MW OTEC plant [48]. T_{surf} and ΔT are the SST and temperature differences between the surface (e.g., 20 m) and deep water (e.g., 1000 m). The turbo generator efficiency (ε_{tg}) is 0.75 [5]. In Eq (4), the first term represents the gross power potential, which is proportional to the temperature difference squared (ΔT^2) and scaled by system and fluid parameters, including cold/warm water flow rates, seawater density, specific heat capacity, and the efficiency of the turbo-generator. The power consumption terms account for about 30 % of the gross OTEC power with the design condition of $\Delta T_{\text{design}} = 20^\circ\text{C}$ [23]. Specifically, the second term represents fixed parasitic losses, which are typically associated with maintaining circulation through the system and are estimated to consume approximately 18 % of the gross power at design conditions. The third term captures variable parasitic losses that scale with the warm-to-cold flow rate ratio (γ) and are associated with pumping requirements and frictional effects, increasing nonlinearly as the system deviates from the design configuration. This term includes an empirical exponent (2.75) that reflects the scaling of friction and other operational inefficiencies. The resulting P_{net} is utilized to characterize the OTEC resources around Kailua-Kona, Hawaii, in this study.

This study employs a simplified net power estimation based on fixed system design parameters. However, recent research has emphasized the sensitivity of OTEC performance to a range of system-level factors. For instance, Rasgianti et al. [49] conducted a comprehensive sensitivity analysis using in situ temperature profiles and found that working fluid selection can significantly affect net power output and thermodynamic efficiency. Their findings suggest that static design assumptions may overlook critical dependencies. To enhance the accuracy and applicability of OTEC resource assessments, future modeling efforts should incorporate parameterized or dynamic formulations that account for variable system configurations such as intake depth, discharge strategy, and fluid properties. Incorporating such factors would improve the accuracy and adaptability of OTEC resource assessments for site selection, design optimization, and techno-economic evaluations under diverse operating conditions.

3. Results and discussion

In this section, we validate the model results with observations for 10 years (2012–2021) and analyze the high-resolution model outputs to understand the characteristics of the ocean temperature around Kailua-Kona, Hawaii. We also characterize the OTEC power resources using the model outputs to find optimal locations for OTEC operation. Lastly, the model is used to investigate the impact of the OTEC discharge on the ocean condition (e.g., ocean temperature) after power generation. The experiment allows us to analyze the potential environmental impacts due to OTEC operation.

3.1. Temperature characteristics around Kailua-Kona, Hawaii

Fig. 2 presents the vertical temperature profiles for both observed (black lines) and modeled (red lines) data at the 15 different locations. A comparison of these results indicates good agreement between the observed and modeled temperatures, showing a mean R of 0.99, RMSE of 0.50 °C, and bias of −0.13 °C throughout the different locations and times. Therefore, it establishes confidence in the model's ability to accurately capture the vertical temperature variations. The temperature profiles in Fig. 2 exhibit similar trends regardless of the locations and times. Surface temperatures are generally above 25 °C, and a rapid decrease in temperature is observed within the upper 500 m of the water column, showing the presence of a thermocline where temperatures drop below 10 °C. At a depth of 1000 m, water temperatures approach or fall below 5 °C. Consequently, the temperature differences between the surface and deep waters (below 1000 m) exceed 20 °C in the ocean near Kailua-Kona, Hawaii, creating favorable ocean conditions for OTEC power generation [50–52].

Fig. 3(a) illustrates the time histories of the spatial mean SST (seven-day running mean) for the observed and modeled data over the 10-year simulation period within the domain outlined in Fig. 1(c). The model accurately captures the interannual and seasonal variations in the SST with R of 0.93, an RMSE of 0.48 °C, and a bias of 0.20 °C, validating its effectiveness for further analyzing the temperature characteristics

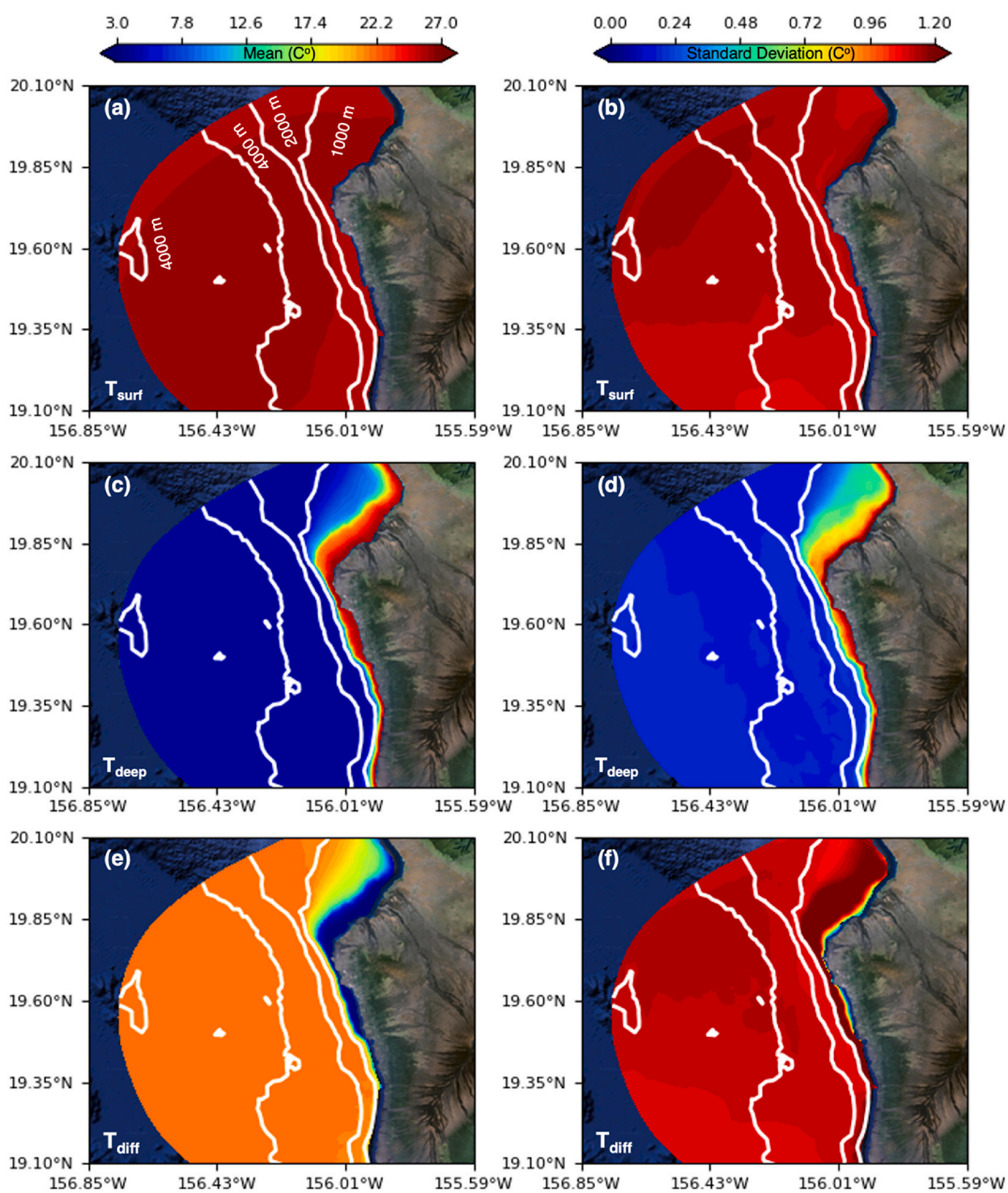

Fig. 4. Two-dimensional maps of the mean (first column) and standard deviation (second column) of the water temperatures from 2012 to 2021. The first and second rows represent the statistics of the temperature at water depths of 20 m (T_{surf}) and 1000 m or the bottom temperature if it is shallower than 1000 m (T_{deep}), respectively. The third row shows the difference in the temperatures at depths of 20 and 1000 m (T_{diff}). The white contour lines in each plot indicate the 1000, 2000, and 4000 m isobaths.

around Kailua-Kona, Hawaii. Fig. 3(b) depicts the monthly mean SST for each year based on the model results in Fig. 3(a), revealing a clear seasonal pattern in the SST around Kona throughout the target period. The data indicate that the SST reaches its peak during the summer months (May to October) and its lowest value during the winter months (October to April). Notably, the summers of 2015 and 2019 exhibit significantly higher SSTs compared to other years, which has also been reported by previous studies [34,53]. Maximum SSTs of 29.17 °C and 29.1 °C are observed in 2015 and 2019, respectively, while 2012 experiences a maximum SST of 26.45 °C, showing a temperature difference of approximately 2.7 °C from 2015. The elevated summer SSTs in 2015 and 2019 can be attributed to reduced wind conditions and large-scale climate phenomena such as the NPGO, ENSO, and PDO, as discussed by Gove et al. [34]. During winter, the minimum SST of 24.33 °C was observed in 2013, compared to 25.20 °C in 2014, indicating a temperature difference of about 1.1 °C between the two years. Further, the interannual SST difference is more pronounced in summer (2.7 °C) compared to winter (1.1 °C). Seasonal variability varies across the years, with the largest seasonal SST difference (maximum summer temperature minus minimum winter temperature) of 4.71 °C observed in 2019, and the smallest difference of 1.91 °C in 2012. Fig. 3(c) presents the yearly mean SST as a bar graph, showing a noticeable increase from 25.4 °C in 2012 to 26.84 °C in 2015. Post-2015, the SST remains elevated, ranging from 26.46 °C to 26.87 °C until 2019, followed by a decline to 26.19 °C by 2021. Overall, the SSTs around Kailua-Kona exhibit high variability on different time scales, driven by local wind conditions and large-scale climate phenomena (NPGO, ENSO, and PDO) [34]. Given that OTEC power generation heavily relies on the ocean temperature, it is crucial to investigate how these temperature variations alter the OTEC power output, which is discussed in Section 3.2.

Because the OTEC power is extracted using the difference in the temperatures of surface and deep waters to generate power, we investigate the temperature fields at different depths using the model outputs. Fig. 4(a) presents the 10-year mean temperature of about 26 °C at a depth of 20 m (T_{surf}) from 2012 to 2021, extending from the coast to the open ocean. The standard deviations of T_{surf}, as depicted in Fig. 4(b), are homogenous across the model domain, ranging from 1.1 °C to 1.2 °C. The 10-year mean temperature at a depth of 1000 m or the bottom temperature, if the depth is shallower than 1000 m (T_{deep}), exhibits distinct patterns as a function of the water depth. Fig. 4(c) illustrates that in regions deeper than 1000 m, the mean T_{deep} is almost uniform at approximately 4 °C. In shallower areas (<1000 m), the bottom water

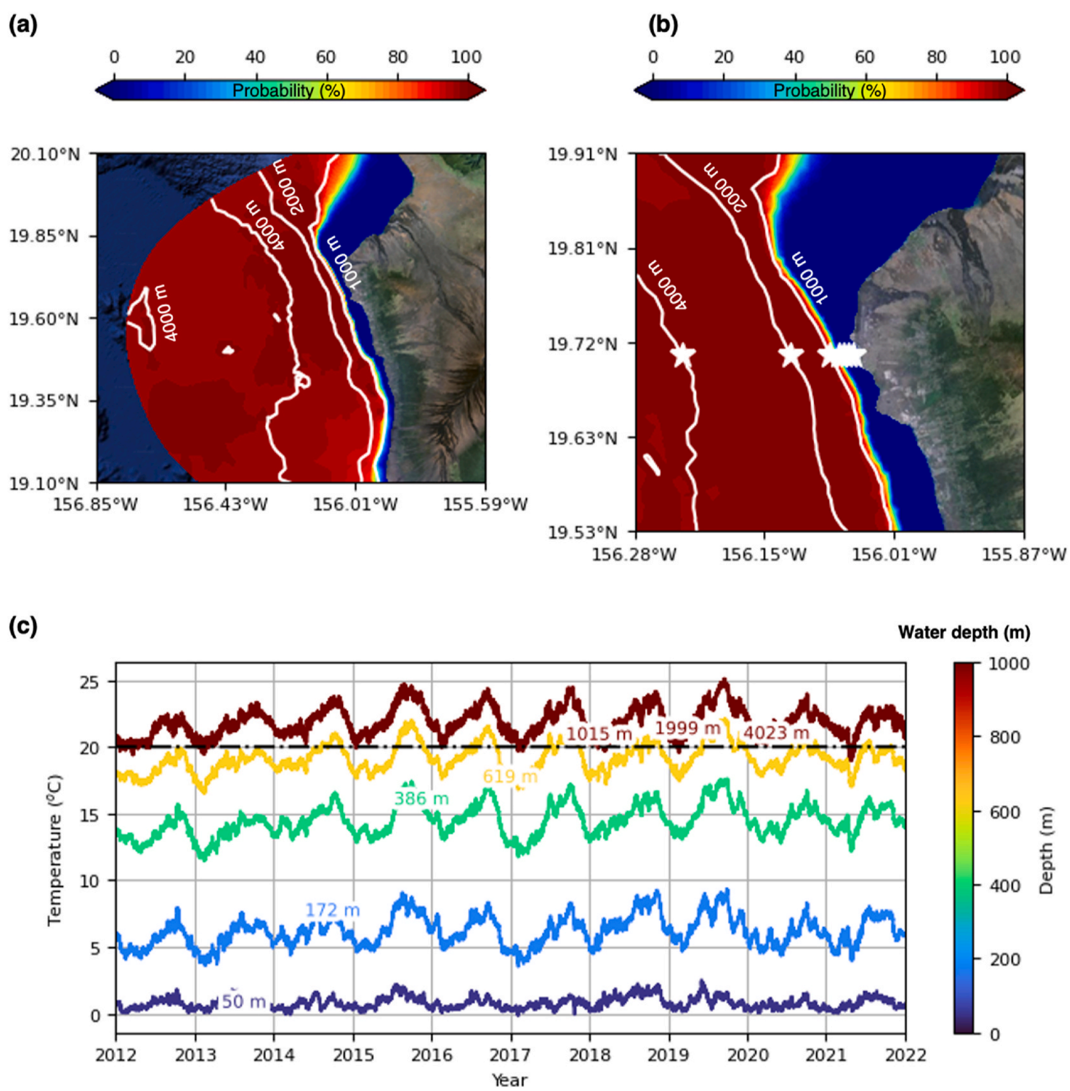

Fig. 5. (a) Two-dimensional map of the probability (%) of T_{diff} exceeding 20 °C. The white contour lines in each plot indicate the 1000, 2000, and 4000 m isobaths. (b) Magnified view of (a) showing the locations of the selected points (white stars) around Kailua-Kona for the time histories of T_{diff}. (c) Time histories of T_{diff} at the different locations indicated by the white starts in (b). The line colors represent different water depths at each location. The dashed line indicates the temperature of 20 °C. (For interpretation of the references to color in this figure legend, the reader is referred to the Web version of this article.)

temperatures rise when moving towards the coast, reaching up to 26 °C, mirroring the surface temperatures because of the well-mixed water columns in the shallow regions. The standard deviation of T_{deep}, shown in Fig. 4(d), indicates low variability (0.16 °C) in deeper waters, while the shallow areas (<1000 m) exhibit higher standard deviations of up to 1.2 °C near the coast, following the surface temperature characteristics. Because of the different spatial characteristics of T_{surf} and T_{deep}, the differences in the temperatures of the surface and deep waters (T_{diff}) display distinct spatial patterns depending on the water depth, as shown in Fig. 4(e). In shallow waters (<1000 m), T_{diff} is below 20 °C and approaches zero in well-mixed waters near the coast. In deeper waters (>1000 m), T_{diff} remains nearly uniform at around 22 °C, providing favorable conditions for OTEC power extraction. The standard deviation of T_{diff} is almost zero near the coast, while it ranges from 1 °C to 1.2 °C in other areas, as shown in Fig. 4(f). The high variability of T_{diff} is primarily influenced by T_{surf} because of the low variability of T_{deep}, as illustrated in Fig. 4(d).

Fig. 5(a) presents a two-dimensional map illustrating the probability (%) of T_{diff} exceeding 20 °C for a 10-year period. In areas where the water depth is deeper than 1000 m, T_{diff} is above 20 °C most of the time, with exceedance probabilities ranging from 92 % to 98 %. Conversely, in regions shallower than 1000 m, the probability of T_{diff} exceeding 20 °C is close to zero in most areas. To further investigate the temporal behavior of T_{diff}, we analyze time series at selected locations. Fig. 5(b) provides a magnified view of the core study area, marking the selected locations (white stars) used for time series analysis in Fig. 5(c). These points represent a range of water depths to examine how T_{diff} varies at different locations and depths. Fig. 5 (c) depicts the time histories of T_{diff} at different locations showing various water depths from 50 to 4000 m. Over the 10-year period, the temporal variations in T_{diff} are similar at depths ranging from 1000 to 4000 m, indicating consistent temperature characteristics in the deep ocean. At a depth of around 600 m, T_{diff} fluctuates around 20 °C because of the seasonality of ocean temperatures. In shallower regions (~50 m), T_{diff} remains close to zero over time, reflecting the well-mixed water columns in these areas. The high-resolution model results offer detailed insights into the ocean temperature characteristics from the coast to the open ocean. Global-scale models are often limited in providing information for shallow depths (<1000 m) because of their coarse grid resolution, resulting in a lack of data for many coastal and island regions with shallower waters [21]. Therefore, the high-resolution data in Figs. 4 and 5 are valuable for identifying the spatiotemporal patterns of T_{diff}, which are essential for determining feasible locations for OTEC plants and characterizing OTEC resources depending on the temperature variability.

3.2. OTEC resource characterization

In this section, we utilize the validated model results to characterize the OTEC power resources at Kailua-Kona, Hawaii. The OTEC power is estimated using the temperature fields and parameters for a 100 MW OTEC plant [e.g., Eq. (4)], as described in Section 2.3.

Fig. 6(a) presents 2D maps of the 10-year mean (from 2012 to 2021) net OTEC power based on Eq. (4). Spatially, the net OTEC power is negligible near the coast because of the small T_{diff}, as discussed for the results presented in Fig. 5. The net OTEC power increases with depth, reaching up to 84 MW at a water depth of 500 m. A high gradient of OTEC power is observed around this depth. Beyond 1000 m, the net OTEC power remains consistent throughout the model domain, averaging about 130 MW. Fig. 6(b) shows the probabilities of the mean net OTEC power exceeding 100 MW, reflecting the target OTEC capacity. The probability exceeds 95 % in areas where the water depth is greater than 1000 m. Conversely, in the areas with depths shallower than 1000 m, the probability approaches zero. This indicates that to achieve the target OTEC capacity of 100 MW, the water depth must exceed 1000 m. The Annual Energy Production (AEP) represents the annual energy output by the 100 MW OTEC plant. Fig. 6(c) depicts the yearly mean AEP for 100 MW OTEC operation over 10 years from 2012 to 2021. In areas where the water depth is greater than 1000 m, the AEP can reach up to 1.2 TWh/year, which has the potential to power approximately 112,686 homes based on a yearly mean household electricity consumption of 10,649 kWh [54].

In addition to analyzing the spatial distribution of the net OTEC power, specific locations were selected to examine the temporal variation in OTEC power. Three locations were identified based on favorable conditions for OTEC operations, including proximity to the coast (≤10 km) and a high probability (≥95 %) of the mean net OTEC power exceeding 100 MW. The locations of these points are presented in Fig. 7 (a). Fig. 7(b) shows the monthly climatology of the net OTEC power at the three different locations. The seasonal variations and magnitudes of OTEC power are similar across these locations, with the highest net OTEC power observed during the summer, peaking at 150 MW in September. In contrast, the lowest net OTEC power occurs during the winter, reaching a minimum of 112 MW in February. These temporal variations in the net OTEC power correlate with the SST patterns shown in Fig. 3, emphasizing the significant role of the ocean temperature in OTEC power generation. Generally, these seasonal fluctuations in OTEC power align with energy demand, with the highest potential power production in the summer months in tropical locations like Hawaii when air conditioning usage increases, which makes OTEC power a promising renewable energy source. Fig. 7(c) presents the AEP for each year at the three different locations. Although the annual variations in the AEP are

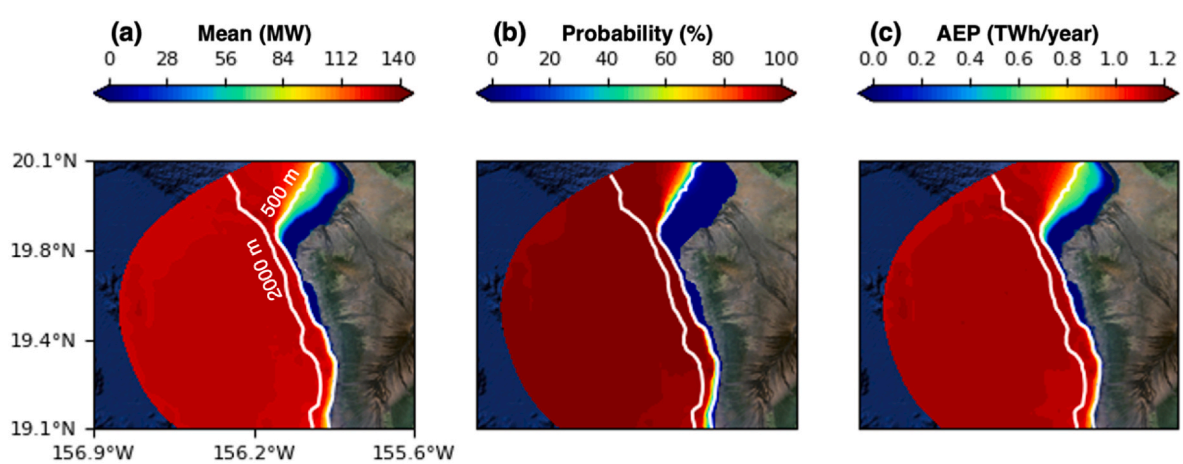

Fig. 6. Two-dimensional maps of the (a) mean, (b) probability (exceeding 100 MW), and (c) annual energy production of the net power from 100 MW OTEC operation.

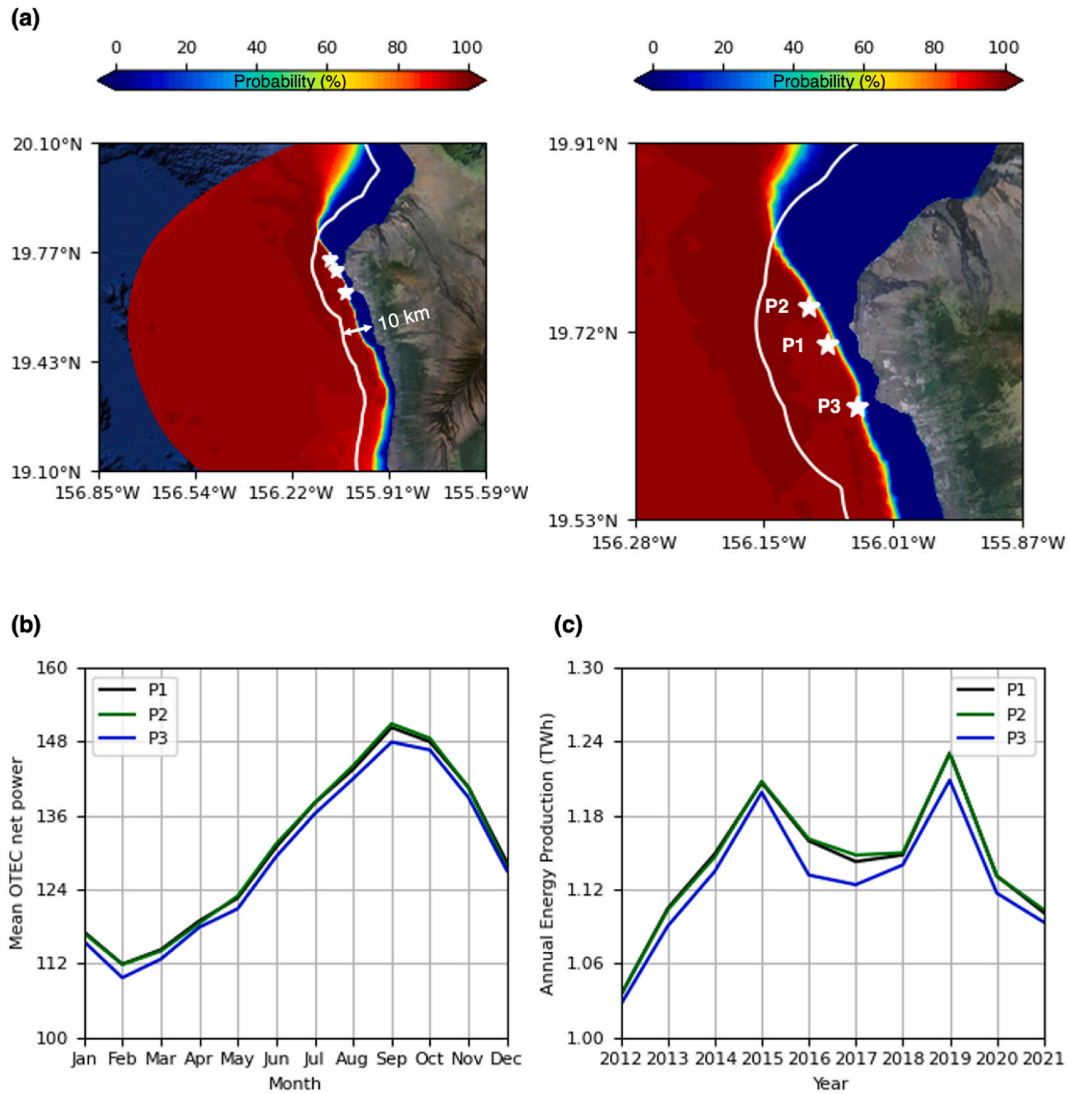

Fig. 7. (a) Locations of points selected for the temporal analysis of the OTEC power. The white line indicates the 10 km distance to the coast. Time histories of the (b) monthly mean net OTEC power and (c) AEP at the three locations.

similar across these locations, P3 shows a lower magnitude compared to the others. The interannual variability in the AEP is evident, reflecting the interannual SST variability over the 10 years. The lowest AEP of 1.03 TWh is recorded in 2012, while the highest AEP of 1.23 TWh is in 2019, indicating a difference of 0.2 TWh. Despite a noticeable temporal variability in OTEC power around the Kona coast, it is evident that OTEC is a valuable energy source with the capacity to power at least 100,000 homes annually at a single location based on yearly energy consumption [54]. Overall, the variations in OTEC power are heavily influenced by the SST variability because deep water temperatures remain relatively constant over time (as indicated by the low standard deviation in Fig. 4) around Kailua-Kona, Hawaii. Since the SST is significantly affected by not only heat flux and wind conditions but also large-scale climate phenomena (NPGO, ENSO, and PDO) [34], as discussed for the results in Fig. 3, advanced resource characterizations for and operation plans of the OTEC should incorporate and consider the climate variability including recent climate change.

3.3. Mixed water discharge from the OTEC plant

After OTEC power generation, warm surface water and cold deep water are mixed and discharged into the ocean ([28,29]; Taguchi et al., 1997; [26]). This process can alter the distributions of the temperature, salinity, and nutrients in the ambient ocean water around the OTEC plant, potentially affecting marine ecosystems and OTEC resources [10, 28,55]. Therefore, it is crucial to investigate the impact of the discharge on the ocean conditions. Previous studies using numerical models have considered different discharge depths ranging from 70 m to 500 m to analyze the influence of mixed water discharge from OTEC plants around Martinique [55] and Hawaii [48]. For Hawaii specifically, recommended discharge depths typically fall between 90 and 115 m, based on local mixed layer depths and light penetration levels [28]. In this study, we adopt a discharge depth of 100 m to reflect these recommendations. A mixed discharge flow rate of 300 m^3/s at a temperature of 10 °C is used to represent a realistic scenario for a 100 MW OTEC plant, which is comparable with values reported by Grandelli et al. [48]. The selected discharge temperature falls within the range (8–16.9 °C) used in previous modeling studies ([55]; Wang et al., 2017). The discharge is implemented as a vertically distributed influx without directional momentum, following established approaches for simulating far-field thermal impacts ([4]; Wang et al., 2017). Although near-field mixing dynamics are not resolved, this configuration is appropriate for assessing long-term, far-field thermal effects of OTEC discharge.

Fig. 8 shows the 10-year mean temperature changes caused by the mixed water discharges from the operation of the three OTEC plants at the same time. The thermal impacts of the mixed water discharges are

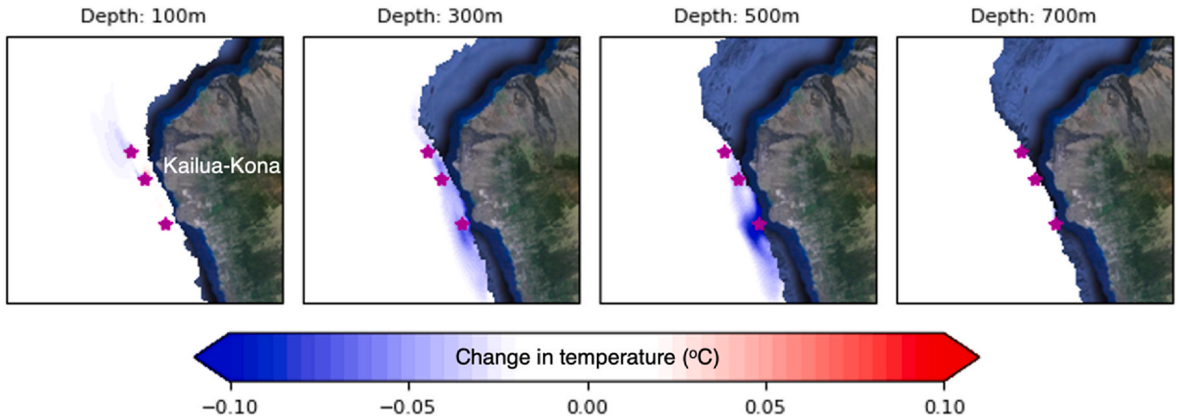

Fig. 8. The 10-year mean temperature changes due to the mixed water discharge from three OTEC plants (magenta stars). The magenta stars indicate the locations of the three OTEC discharges. Each frame represents a 2D map of the change in the temperature at different depths from 100 m to 700 m. The blue color means a decrease in temperature due to the mixed water discharge. (For interpretation of the references to color in this figure legend, the reader is referred to the Web version of this article.)

minimal at the discharge depth (100 m), showing negligible temperature changes. However, at water depths of 300 and 500 m, the mixed water discharge decreases the water temperature by up to 0.1 °C. This occurs because the released mixed water has a higher density than the ambient water due to its colder temperature at the discharge depth, causing it to sink to deeper levels (e.g., 300 and 500 m), where it has a more noticeable impact than at a shallower depth (e.g., 100 m). Given that a temperature change of 3 °C is a critical threshold for thermal impact [27,55], the temperature change (up to 0.1 °C) corresponding to current OTEC configurations can be deemed to have a negligible impact on the ocean conditions. Additionally, previous studies reported that a 0.3 °C temperature variation has a negligible impact on marine ecosystems [55]. At greater depths (e.g., 700 m), the impact of the mixed water discharge is negligible, showing almost no temperature change. The minor changes in ambient ocean water temperature at all depths suggest that OTEC power operations, which rely on warm shallow water and cold deep water, are not significantly altered by the mixed water discharge.

Overall, the impacts of mixed water discharge from the three OTEC plants on ocean conditions are minor for both the marine ecosystem and OTEC power resources. However, it is important to recognize that the thermal effects of discharge can vary significantly with the scale and configuration of the OTEC operation. For example, global-scale OTEC simulations have shown temperature changes ranging from −4 °C near the surface (e.g., at 55 m depth) to +10 °C at deeper levels (e.g., around 1160 m), highlighting the potential for substantial subsurface thermal alterations under large-scale deployment scenarios [4]. In addition, the present study assumes steady-state flow rates and temperatures for the discharge and does not include coupling with biogeochemical or ecological processes. Consequently, the model does not account for potential changes in nutrient dynamics, dissolved oxygen, or biological productivity by the mixed water discharges from OTEC plants. Addressing these limitations will require the development of fully coupled hydrodynamic-biogeochemical modeling frameworks capable of capturing the feedback between thermal perturbations and marine ecosystem processes.

4. Conclusion

This study presents a high-resolution, decade-long characterization of OTEC resources around Kona, Hawaii, using an unstructured-grid 3D ocean model. The results demonstrate that the spatial and temporal variability of thermal gradients shaped by regional bathymetry and modulated by large-scale climate modes such as ENSO, PDO, and NPGO plays a critical role in determining OTEC energy potential. The model captures fine-scale oceanographic features that are often missed by coarse-resolution models or limited observational datasets, enabling more accurate and site-specific assessments of the temperature differentials essential for OTEC performance. Key findings from the power analysis for a 100 MW OTEC plant include.

- In areas where water depth exceeds 1000 m, the 10-year mean net OTEC power output is approximately 130 MW, with a greater than 95 % probability of achieving the design capacity for the 10-year period.
- Peak net OTEC power (up to 150 MW) occurs during summer months, coinciding with increased regional energy demand from air conditioning.
- Theoretical AEP in deep-water zones (depth >1000 m) can reach up to 1.2 TWh/year—enough to power over 112,000 homes, demonstrating the practical feasibility of OTEC as a renewable energy solution for Hawaii.
- In contrast, OTEC power potential is negligible in shallower areas (depth <500 m), emphasizing the detailed resource characterization around the coast.

We also conduct a numerical experiment to investigate the impact of mixed water discharge from three OTEC plants on the ocean conditions around Kailua-Kona, Hawaii. Model results show that the thermal impacts of mixed water discharge are minor for marine ecosystems and OTEC resources. Nevertheless, sensitivity experiments with various OTEC operation scales and discharge parameters are recommended to further understand various aspects of mixed water discharges.

Overall, the study underscores the potential of OTEC as a valuable renewable energy source, particularly in regions with large sea surface and bottom temperature differences and suitable water depths. The high-resolution ocean model provides critical insights into the spatio-temporal patterns of ocean temperatures, aiding in the strategic planning and optimal placement of OTEC facilities. Building on the validated high-resolution modeling framework developed in this study, future research can apply this approach to other coastal and island regions with favorable ocean thermal structures. Many tropical and subtropical locations including areas in the Caribbean and the Western Pacific exhibit strong vertical temperature gradients and energy security challenges similar to those in Hawaii. Applying this framework elsewhere would enable site-specific OTEC assessments that account for local bathymetry, stratification patterns, and climate variability, ultimately supporting more globally distributed feasibility studies and informed decision-making for OTEC deployment. In addition, future work should investigate how OTEC operations influence nutrient availability, phytoplankton growth, and vertical stratification across both seasonal and interannual timescales. Further model validation and targeted sensitivity experiments that explore a range of operational scenarios, including different scales of OTEC deployment, intake/discharge parameters, and background climate conditions are essential for advancing our understanding of the environmental impacts of OTEC.

CRediT authorship contribution statement

Kyungmin Park: Writing – review & editing, Writing – original draft, Visualization, Validation, Software, Methodology, Investigation, Formal analysis, Data curation, Conceptualization. **Zhaoqing Yang:** Writing – review & editing, Supervision. **Andrea E. Copping:** Writing – review & editing, Funding acquisition. **Fadia Ticona Rollano:** Writing – review & editing.

Declaration of competing interest

The authors declare that they have no known competing financial interests or personal relationships that could have appeared to influence the work reported in this paper.

Acknowledgments

This study was funded by the U.S. Department of Energy, Office of Energy Efficiency and Renewable Energy, Water Power Technologies Office under contract DE-AC05-76RL01830 at the Pacific Northwest National Laboratory (PNNL). All model simulations were performed using PNNL's Institutional Computing facility and NREL's Kestrel Computing System.

References

[1] A. Etemadi, A. Emdadi, O. AsefAfshar, Y. Emami, Electricity generation by the ocean thermal energy, Energy Proc. 12 (2011) 936–943.
[2] F. Sinama, F. Lucas, F.O. Garde, Modeling of ocean thermal energy conversion (OTEC) plant in Reunion island, Energy Sustainability 43949 (2010) 929–936.
[3] O. Edenhofer, R. Pichs-Madruga, Y. Sokona, K. Seyboth, S. Kadner, T. Zwickel, P. Eickemeier, G. Hansen, S. Schloemer, C. von Stechow, Renewable Energy Sources and Climate Change Mitigation: Special Report of the Intergovernmental Panel on Climate Change, Cambridge University Press, 2011.
[4] K. Rajagopalan, G.C. Nihous, An assessment of global ocean thermal energy conversion resources with a high-resolution ocean general circulation model, J. Energy Resour. Technol. 135 (4) (2013) 041202.
[5] T. Du, Z. Jing, L. Wu, H. Wang, Z. Chen, X. Ma, B. Gan, H. Yang, Growth of ocean thermal energy conversion resources under greenhouse warming regulated by Oceanic eddies, Nat. Commun. 13 (1) (2022) 7249.
[6] R. Fujita, A.C. Markham, J.E. Diaz Diaz, J.R. Martinez Garcia, C. Scarborough, P. Greenfield, P. Black, S.E. Aguilera, Revisiting ocean thermal energy conversion, Mar. Pol. 36 (2) (2012) 463–465.
[7] E.P. Garduño-Ruiz, R. Silva, Y. Rodríguez-Cueto, A. García-Huante, J. Olmedo-González, M.L. Martínez, A. Wojtarowski, R. Martell-Dubois, S. Cerdeira-Estrada, Criteria for optimal site selection for ocean thermal energy conversion (OTEC) plants in Mexico, Energies 14 (2021) 2121.
[8] L. Aresti, P. Christodoulides, C. Michailides, T. Onoufriou, Reviewing the energy, environment, and economy prospects of ocean thermal energy conversion (OTEC) systems, Sustain. Energy Technol. Assessments 60 (2023) 103459.
[9] A. Hossain, A. Azhim, A.B. Jaafar, M.N. Musa, S.A. Zaki, D. Noor Fazreen, Ocean thermal energy conversion: the promise of a clean future, in: 2013 IEEE Conference on Clean Energy and Technology (CEAT), 2013, pp. 23–26.
[10] K. Rajagopalan, G.C. Nihous, Estimates of global ocean thermal energy conversion (OTEC) resources using an ocean general circulation model, Renew. Energy 50 (2013) 532–540.
[11] W. Liu, X. Xu, F. Chen, Y. Liu, S. Li, L. Liu, Y. Chen, A review of research on the closed thermodynamic cycles of ocean thermal energy conversion, Renew. Sustain. Energy Rev. 119 (2020) 109581.
[12] C. Zhang, Z. Wu, J. Wang, C. Ding, T. Gao, Y. Chen, Thermodynamic performance of a radial-inflow turbine for ocean thermal energy conversion using ammonia, Renew. Energy 202 (2023) 907–920.
[13] A. Liponi, A. Baccioli, D. Vera, L. Ferrari, Seawater desalination through reverse osmosis driven by ocean thermal energy conversion plant: thermodynamic and economic feasibility, Appl. Therm. Eng. 213 (2022) 118694.
[14] F. Yilmaz, M. Ozturk, R. Selbas, Design and performance assessment of an OTEC driven combined plant for producing power, freshwater, and compressed hydrogen, Int. J. Hydrogen Energy 58 (2024) 688–697.
[15] D. Li, Z. Deng, C. Zhang, Thermodynamic process control of compression-assisted absorption refrigeration using ocean thermal energy, Renew. Energy 222 (2024) 119903.
[16] Y. Ding, F. Duan, S. Tabeta, Site assessment of multi-purpose offshore platform with OTEC in east and southeast Asia, in: OCEANS 2022, Hampton Roads, 2022, pp. 1–6.
[17] Z. Tian, X. Zou, Y. Zhang, W. Gao, W. Chen, H. Peng, 4E analyses and multi-objective optimization for an innovative solar-ocean thermal energy conversion/air conditioning system, J. Clean. Prod. 414 (2023) 137532.
[18] C. Fan, Z. Wu, J. Wang, Y. Chen, C. Zhang, Thermodynamic process control of ocean thermal energy conversion, Renew. Energy 210 (2023) 810–821.
[19] A. Devis-Morales, R. Montoya-Sánchez, A.F. Osorio, L.J. Otero-Díaz, Ocean thermal energy resources in Colombia, Renew. Energy 66 (2014) 759–769.
[20] D.E. Lennard, The viability and best locations for ocean thermal energy conversion systems around the world, Renew. Energy 6 (3) (1995) 359–365.
[21] J.H. VanZwieten, L.T. Rauchenstein, L. Lee, An assessment of Florida's ocean thermal energy conversion (OTEC) resource, Renew. Sustain. Energy Rev. 75 (2017) 683–691.
[22] Y. Jia, G.C. Nihous, K. Rajagopalan, An evaluation of the large-scale implementation of ocean thermal energy conversion (OTEC) using an ocean general circulation model with low-complexity atmospheric feedback effects, J. Mar. Sci. Eng. 6 (1) (2018) 12.
[23] G.C. Nihous, A preliminary assessment of ocean thermal energy conversion (OTEC) resources, J. Energy Resour. Technol. 129 (1) (2007) 10–17.
[24] G.C. Nihous, Mapping available ocean thermal energy conversion resources around the main Hawaiian islands with state-of-the-art tools, J. Renew. Sustain. Energy 2 (4) (2010) 043101.
[25] A.F. Osorio, S. Ortega, S. Arango-Aramburo, Assessment of the marine power potential in Colombia, Renew. Sustain. Energy Rev. 53 (2016) 966–977.
[26] Z. Wang, S. Tabeta, Y. Kitakoji, S. Okamura, Numerical simulations for behavior of discharged water from ocean thermal energy conversion plant, 2016 Techno-Ocean (Techno-Ocean) (2016) 225–234.
[27] A. Bordbar, K. Georgoulas, Y.M. Dai, S. Michele, F. Roberts, N. Carter, Y.C. Lee, Waterbodies thermal energy based systems interactions with marine environment—A review, Energy Rep. 9 (2023) 5269–5286.
[28] C.M. Comfort, L. Vega, Environmental assessment for ocean thermal energy conversion in Hawaii: available data and a protocol for baseline monitoring. OCEANS'11 MTS/IEEE KONA, 2011, pp. 1–8.
[29] G. Nihous, A preliminary investigation of the effect of ocean thermal energy conversion (OTEC) effluent discharge options on global OTEC resources, J. Mar. Sci. Eng. 6 (1) (2018) 25.
[30] H.T. Hewitt, M.J. Bell, E.P. Chassignet, A. Czaja, D. Ferreira, S.M. Griffies, P. Hyder, J.L. McClean, A.L. New, M.J. Roberts, Will high-resolution global ocean models benefit coupled predictions on short-range to climate timescales? Ocean Model. (Oxf.) 120 (2017) 120–136.
[31] T. Rackow, D.V. Sein, T. Semmler, S. Danilov, N.V. Koldunov, D. Sidorenko, Q. Wang, T. Jung, Sensitivity of deep ocean biases to horizontal resolution in prototype CMIP6 simulations with AWI-CM1.0, Geosci. Model Dev. (GMD) 12 (2019) 2635–2656.
[32] K. Rajagopalan, G.C. Nihous, An assessment of global ocean thermal energy conversion resources under broad geographical constraints, J. Renew. Sustain. Energy 5 (6) (2013).
[33] Hawaii State Energy Office, Hawaii energy facts and figures. https://energy.hawaii.gov/wp-content/uploads/2020/11/HSEO_FactsAndFigures-2020.pdf, 2020.
[34] J.M. Gove, Lecky, W.J. Walsh, R.J. Ingram, K. Leong, I.D. Williams, J.J. Polovina, J. Maynard, R. Whittier, K.L. Kramer, E. Schemmel, West Hawai'I Integrated Ecosystem Assessment Ecosystem Status Report, PIFSC Special Publication, 2019. SP-19-001.
[35] M.J. McPhaden, S.E. Zebiak, M.H. Glantz, ENSO as an integrating concept in Earth science, Sci. Technol. Humanit. 314 (5806) (2006) 1740–1745.
[36] N.J. Mantua, S.R. Hare, Y. Zhang, J.M. Wallace, R.C. Francis, A Pacific interdecadal climate oscillation with impacts on salmon production, Bull. Am. Meteorol. Soc. 78 (6) (1997) 1069–1079.
[37] E. Di Lorenzo, N. Schneider, K.M. Cobb, P.J. Franks, K. Chhak, A.J. Miller, S. J. Bograd, North Pacific gyre oscillation links ocean climate and ecosystem change, Geophys. Res. Lett. 35 (8) (2008).
[38] Y.J. Zhang, F. Ye, E.V. Stanev, S. Grashorn, Seamless cross-scale modeling with SCHISM, Ocean Model. (Oxf.) 102 (2016) 64–81.
[39] F. Ye, Y.J. Zhang, R. He, Z. Wang, H.V. Wang, J. Du, Third-order WENO transport scheme for simulating the baroclinic eddying ocean on an unstructured grid, Ocean Model. (Oxf.) 143 (2019) 101466.
[40] L. Umlauf, H. Burchard, A generic length-scale equation for geophysical turbulence models, J. Mar. Res. 61 (2) (2003).
[41] Y.J. Zhang, J. Anderson, K. Park, C.H. Wu, S. Wipperfurth, E. Anderson, S. Pe'eri, D. Beletsky, D. Titze, E. Di Lorenzo, S. Moghimi, Debunking common myths in coastal circulation modeling, Ocean Model. (Oxf.) 190 (2024) 102401.
[42] P.A. Hwang, High-wind drag coefficient and whitecap coverage derived from microwave radiometer observations in tropical cyclones, J. Phys. Oceanogr. 48 (10) (2018) 2221–2232.
[43] F.H. Lyard, D.J. Allain, M. Cancet, L. Carrère, N. Picot, FES2014 global ocean tide atlas: design and performance, Ocean Sci. 17 (3) (2021) 615–649.
[44] J.M. Lellouche, E. Greiner, O. Le Galloudec, G. Garric, C. Regnier, M. Drevillon, M. Benkiran, C.E. Testut, R. Bourdalle-Badie, F. Gasparin, O. Hernandez, Recent updates to the copernicus marine service global ocean monitoring and forecasting real-time 1/12° high-resolution system, Ocean Sci. 14 (5) (2018) 1093–1126.

[45] S. Saha, S. Moorthi, X. Wu, J. Wang, S. Nadiga, P. Tripp, D. Behringer, Y.-T. Hou, H. Chuang, M. Iredell, M. Ek, J. Meng, R. Yang, M. Peña Mendez, H. van den Dool, Q. Zhang, W. Wang, M. Chen, E. Becker, The NCEP climate forecast system version 2, J. Clim. 27 (2014) 2185–2208.

[46] G.C. Nihous, M.A. Syed, L.A. Vega, Design of a Small OTEC Plant for the Production of Electricity and Fresh Water in a Pacific Island, in: Proceedings of the ASCE International Conference on Ocean Energy Recovery, 1989, pp. 207–216.

[47] L.A. Vega, G.C. Nihous, Design of a 5 MW pre-commercial OTEC plant, Proceedings of Oceanology International '94 5 (1994) 18.

[48] P. Grandelli, G. Rocheleau, J. Hamrick, M. Church, B. Powell, Modeling the Physical and Biochemical Influence of Ocean Thermal Energy Conversion Plant Discharges into Their Adjacent Waters, Makai Ocean Engineering, Inc, 2012. DOE/EE0003638-1.

[49] R.A. Rasgianti, A.D. Nugraha, R.B. Sitanggang, W.W. Pandoe, T.Y. Aprijanto, M. A. Santosa, System parameters sensitivity analysis of ocean thermal energy conversion, Emerging Science Journal 8 (2) (2024).

[50] A.-S. Hamedi, S. Sadeghzadeh, Conceptual design of a 5 MW OTEC power plant in the Oman Sea, Journal of Marine Engineering & Technology 16 (2) (2017) 94–102.

[51] D. Li, J. Yue, L. Zhang, X. Duan, Numerical study on ocean thermal energy conversion system, J. Renew. Sustain. Energy 10 (4) (2018) 044501.

[52] S.M. Masutani, P.K. Takahashi, Ocean thermal energy conversion (OTEC), Oceanography (Wash. D. C.) 22 (609) (2001) 625.

[53] M. Winston, T. Oliver, C. Couch, M.K. Donovan, G.P. Asner, E. Conklin, K. Fuller, B. W. Grady, B. Huntington, K. Kageyama, T.L. Kindinger, Coral taxonomy and local stressors drive bleaching prevalence across the Hawaiian archipelago in 2019, PLoS One 17 (9) (2022) e0269068.

[54] L. Kilcher, M. Fogarty, M. Lawson, Marine Energy in the United States: an Overview of Opportunities, National Renewable Energy Laboratory, 2021. NREL/TP-5700-78773.

[55] M. Giraud, V. Garçon, D. de La Broise, S. L'Helguen, J. Sudre, M. Boye, Potential effects of deep seawater discharge by an ocean thermal energy conversion plant on the marine microorganisms in oligotrophic waters, Sci. Total Environ. 693 (2019) 133491.